CellPress

Cell Stem Cell
Article

Dnmt3a and Dnmt3b Have Overlapping and Distinct Functions in Hematopoietic Stem Cells

Grant A. Challen,[1,8,*] Deqiang Sun,[2,6,8] Allison Mayle,[3,4,8] Mira Jeong,[3,8] Min Luo,[3,5,8] Benjamin Rodriguez,[2,6] Cates Mallaney,[1] Hamza Celik,[1] Liubin Yang,[3] Zheng Xia,[2,6] Sean Cullen,[3] Jonathan Berg,[3,7] Yayun Zheng,[3] Gretchen J. Darlington,[5] Wei Li,[2,6,9] and Margaret A. Goodell[2,3,4,9,*]

[1]Division of Oncology, Section of Molecular Oncology, Department of Internal Medicine, Washington University in St. Louis, St. Louis, MO 63110, USA
[2]Dan L. Duncan Cancer Center, Baylor College of Medicine, Houston, TX 77030, USA
[3]Stem Cell and Regenerative Medicine Center, Department of Pediatrics, Baylor College of Medicine, Houston, TX 77030, USA
[4]Department of Molecular and Human Genetics, Baylor College of Medicine, Houston, Texas 77030, USA
[5]Huffington Center for Aging, Baylor College of Medicine, Houston, TX 77030, USA
[6]Department of Molecular and Cellular Biology, Baylor College of Medicine, Houston, TX 77030, USA
[7]Present address: Department of Genetics, University of North Carolina, Chapel Hill, NC 27599, USA
[8]Co-first author
[9]Co-senior author
*Correspondence: gchallen@dom.wustl.edu (G.A.C.), goodell@bcm.edu (M.A.G.)
http://dx.doi.org/10.1016/j.stem.2014.06.018

SUMMARY

Epigenetic regulation of hematopoietic stem cells (HSCs) ensures lifelong production of blood and bone marrow. Recently, we reported that loss of de novo DNA methyltransferase Dnmt3a results in HSC expansion and impaired differentiation. Here, we report conditional inactivation of Dnmt3b in HSCs either alone or combined with Dnmt3a deletion. Combined loss of *Dnmt3a* and *Dnmt3b* was synergistic, resulting in enhanced HSC self-renewal and a more severe block in differentiation than in *Dnmt3a*-null cells, whereas loss of *Dnmt3b* resulted in a mild phenotype. Although the predominant *Dnmt3b* isoform in adult HSCs is catalytically inactive, its residual activity in *Dnmt3a*-null HSCs can drive some differentiation and generates paradoxical hypermethylation of CpG islands. *Dnmt3a*/*Dnmt3b*-null HSCs displayed activated β-catenin signaling, partly accounting for the differentiation block. These data demonstrate distinct roles for *Dnmt3b* in HSC differentiation and provide insights into complementary de novo methylation patterns governing regulation of HSC fate decisions.

INTRODUCTION

DNA methylation of CpG dinucleotides is a major mode of epigenetic regulation in the vertebrate genome with functions including silencing of repetitive elements, X chromosome inactivation, genomic imprinting, and regulation of gene expression (Jaenisch and Jähner, 1984; Ng and Bird, 1999; Surani, 1998). Of the three catalytic DNA methyltransferase enzymes, Dnmt1, has a higher affinity for hemimethylated DNA than unmethylated DNA (Bestor, 1992), and ablation of *Dnmt1* in embryonic stem cells (ESCs) leads to extensive but nonspecific loss of DNA methylation, leading to the view that *Dnmt1* is a "maintenance" methyltransferase (Lei et al., 1996; Li et al., 1992). Conversely, *Dnmt3a* and *Dnmt3b* act as de novo DNA methyltransferases responsible for the establishment of DNA methylation patterns, predominantly during early development (Hata et al., 2002; Okano et al., 1999). However, *Dnmt3a* and *Dnmt3b* also appear important for the stable inheritance of some DNA methylation, given that a loss of both enzymes in ESCs results in progressive loss of DNA methylation in repetitive and some single-copy elements (Chen et al., 2003).

Although Dnmt3a and Dnmt3b are highly homologous, their biological functions remain unclear. *Dnmt3b*-null mice die at midgestation with multiple developmental defects, and *Dnmt3a*-null mice die shortly after birth (Okano et al., 1999), but their cell-type-specific roles have not been fully elucidated. Compound *Dnmt3a*/*Dnmt3b* double knockout (DKO) embryos arrest shortly after gastrulation (Okano et al., 1999), and DKO ESCs display inefficient differentiation which is increasingly pronounced with extended passage (Chen et al., 2003). In neural stem cells, *Dnmt3a* is required for neurogenesis, given that Dnmt3a-dependent nonproximal promoter methylation regulates expression of neurogenic genes (Wu et al., 2010).

Our group has recently reported that *Dnmt3a* is essential for hematopoietic stem cell (HSC) differentiation, given that *Dnmt3a*-null HSCs show a marked decline in differentiation capacity on a per-HSC basis over serial transplantation, resulting in accumulation of undifferentiated HSCs in the bone marrow (Challen et al., 2012). Moreover, mutations in *DNMT3A* are prevalent in myeloid malignancies (Ley et al., 2010; Walter et al., 2011; Yan et al., 2011) and lymphoid leukemias (Grossmann et al., 2013), consistent with an important function in hematopoiesis. However, no distinct role for *Dnmt3b* has been identified in HSCs or any other adult stem cell. Here, we conditionally ablate *Dnmt3b* alone or in combination with *Dnmt3a* and investigate the functional consequences for HSCs.

RESULTS

Dnmt3s Cooperatively Enable Long-Term HSC Differentiation In Vivo

Similar to *Dnmt3a*, *Dnmt3b* is most highly expressed in long-term HSCs relative to differentiated cells (Figure S1A available online). To investigate the functional role of *Dnmt3b*, we generated conditional KO mice by crossing *Dnmt3b*$^{fl/fl}$ and *Dnmt3a*$^{fl/fl}$ mice (Dodge et al., 2005) with *Mx1*-cre mice in order to generate inducible *Dnmt3b*-KO (3bKO) and *Dnmt3a*/*Dnmt3b* DKO mice. We also compare data from these mice in some cases with that from *Dnmt3a*-KO mice (3aKO; data generated here or from Challen et al., 2012). The function of KO HSCs was examined by competitive transplantation. Two-hundred-fifty HSCs (side population^{+} c-Kit^{+} Lin^{-}Sca-1^{+}) were transplanted into lethally irradiated recipient mice along with 250 × 10^{3} whole-bone-marrow (WBM) cells from genetically distinguishable wild-type (WT) mice (CD45 allelic differences; see the Experimental Procedures). Floxed allele deletion was induced in donor HSCs 4 weeks posttransplantation in order to avoid confounding effects of *Dnmt3* deletion in the niche or a requirement during homing. Control mice throughout this study (unless otherwise specified) consisted of *Dnmt3b*$^{fl/fl}$, *Dnmt3a*$^{fl/fl}$*Dnmt3b*$^{fl/fl}$ (or similarly genetically-matched) littermates that lacked *Mx1*-cre, which were otherwise treated identically, including treatment with polyinosinic-polycytidylic acid (pIpC) in order to control for interferon-mediated effects.

Analysis of peripheral blood chimerism in primary recipients revealed no significant differences in mice transplanted with 3bKO or DKO HSCs in comparison to control HSCs (Figure 1A). Given that 3aKO HSCs also did not exhibit a phenotype in primary transplants (Challen et al., 2012), we performed serial transplantation. HSCs were purified from primary recipients 18 weeks posttransplant, and 250 HSCs were transferred to secondary recipients along with fresh WT competitor WBM cells. Although 3bKO HSCs performed similarly to control HSCs, blood production by DKO HSCs dropped precipitously (Figure 1A), with a dearth of DKO-derived cells in all peripheral blood lineages 16 weeks posttransplant (Figure S1B). In a third round of transplantation, 3bKO HSCs continued to perform similar to control HSCs but with a slight increase in B cell generation (Figure S1B). In contrast, DKO HSCs contributed to peripheral blood only transiently after the third round of transplantation (Figure 1A). These phenotypes are markedly distinct from the 3aKO HSCs, which showed enhanced blood production relative to control cells over four rounds of serial transplantation (Challen et al., 2012).

Dnmt3b Enables Some HSC Differentiation in the Absence of Dnmt3a

Self-renewal was evaluated by enumerating phenotypically defined HSCs regenerated in the bone marrow 18 weeks after each round of transplantation. In primary mice, the numbers of HSCs generated from control and 3bKO was the same, but the number of DKO HSCs was increased significantly (Figure 1B). This behavior was exacerbated in subsequent rounds of transplantation. In secondary recipients, input of 250 control HSCs generated 6,692 ± 675 HSCs, whereas the same input of DKO HSCs generated 305,472 ± 25,144 DKO HSCs. Similarly in tertiary transplants, 250 input control HSCs generated 3,061 ± 965 HSCs, whereas DKO HSCs produced 295,429 ± 37,813 HSCs (Figure S1C). The bone marrow of tertiary mice transplanted with DKO HSCs harbored nearly 50-fold more HSCs than those from control or 3bKO transplanted recipients, with nearly all of the HSCs derived from DKO cells (Figures 1C and S1D) even though these animals were almost devoid of DKO-derived peripheral blood cells (Figure 1A). DKO HSCs show superior self-renewal in comparison to 3aKO with approximately 5-fold more HSCs generated in each round of transplant (Figure 1B). However, unlike 3aKO HSCs, which retain some differentiation capacity even after four rounds of transplantation (Challen et al., 2012), the differentiation of DKO cells is decimated after secondary transfer.

These data show that *Dnmt3b* plays a critical role in enabling differentiation in the absence of *Dnmt3a*. Although loss of *Dnmt3a* alone has a more dramatic effect than loss of *Dnmt3b*, the effect of *Dnmt3b* is evidenced by the comparison between 3aKO and DKO. This concept is underscored when we examine, on a per-HSC basis, the output of differentiation (16-week white blood cell count per ul blood × the percentage test-cell blood chimerism / number of donor-derived HSCs, the "differentiation quotient") versus self-renewal (the number of donor-derived HSCs recovered at end of transplant per original input HSC, the "self-renewal quotient") in each of the genotypes (Figure 1D). The DKO HSCs resemble the 3aKO HSCs in overall behavior, but the kinetics are distinct, with loss of differentiation ability and increase in self-renewal apparent in the first round of transplantation. Moreover, the self-renewal capacity of the DKO HSCs is roughly 5× that of the 3aKO HSCs on a per-cell basis.

This is consistent with the idea that the Dnmt3s serve as a critical regulators at the decision point between HSC differentiation and self-renewal. Analysis of bone marrow progenitors in secondary transplants confirmed that the block in DKO differentiation occurred predominantly at the level of the HSC (Figure S2) with a dearth of all downstream progenitors (Figure 2A). Moreover, DKO HSCs were unable to differentiate well in vitro with cytokine and stromal cell support. HSCs isolated at the end of each round of serial transplantation and cultured in methylcellulose with myeloid differentiation factors revealed a deficit in the number of myeloid colonies produced from DKO HSCs in comparison to transplant-matched control HSCs (Figure 2B). Although DKO HSCs could be serially replated (Figure S2D), the colonies derived after the second plating were comprised of an outgrowth of mast cells (Gr-1^{-}Mac-1^{-}c-Kit^{+}FcεR1^{+}) and not the normal distribution of myeloid colonies (data not shown). No difference was noted between control and 3bKO HSCs in the same assay (Figures 2B and S2D). Genotyping of single-HSC-derived colonies showed efficient excision of floxed alleles (Figures S2E–2G). Coculture of HSCs purified after secondary transplant with OP9 stromal cells revealed a severe block in B cell differentiation of DKO HSCs (Figure 2C) regardless of the concentrations of lymphoid cytokines (IL-7 and Flt3L) or the number of HSCs seeded per well (Figure 2D). These results contrast with 3aKO HSCs, which were capable of robust myeloid and lymphoid differentiation in vitro (Challen et al., 2012) and reinforce the notion that *Dnmt3b* plays a critical role in enabling HSC differentiation, particularly in the absence of *Dnmt3a*.

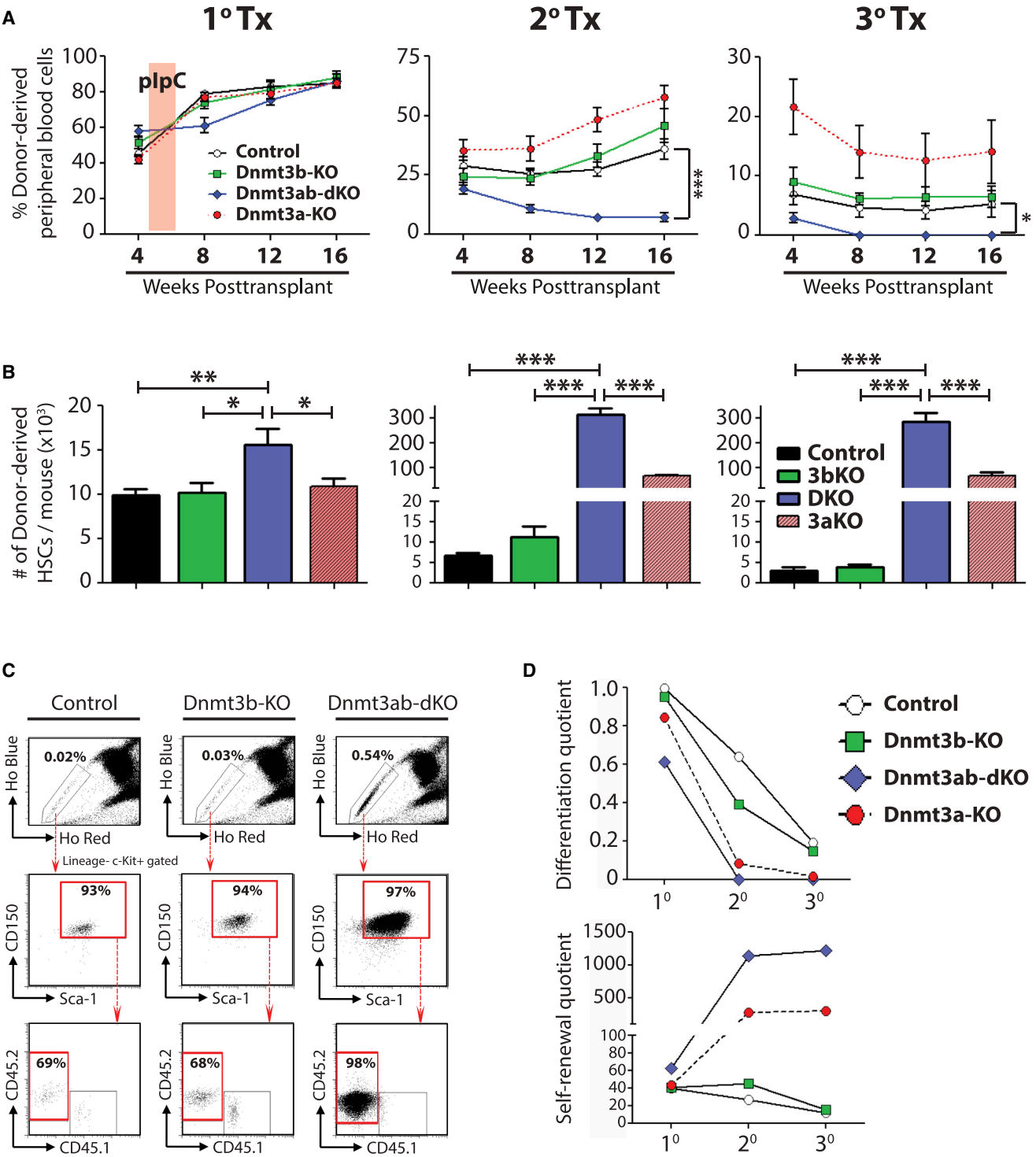

Figure 1. De Novo DNA Methylation Is Required for Long-Term HSC Differentiation In Vivo

(A) Donor-cell-derived peripheral blood chimerism in mice transplanted with control, Dnmt3b-KO (3bKO), or Dnmt3ab-dKO (DKO) HSCs. The previously determined values for Dnmt3a-KO (3aKO) HSCs (Challen et al., 2012) are included for reference in the following panels.

(B) Enumeration of donor-derived HSCs per mouse 18 weeks posttransplant over serial transplantation.

(C) Bone marrow fluorescence-activated cell sorting analysis of tertiary transplanted mice showing accumulation of DKO HSCs.

(E) Differentiation and self-renewal quotients of HSC genotypes over serial transplant. Mean ± SEM values are shown (n = 16–35 recipient mice per genotype). *p < 0.05, **p < 0.01, ***p < 0.001.

See also Figure S1.

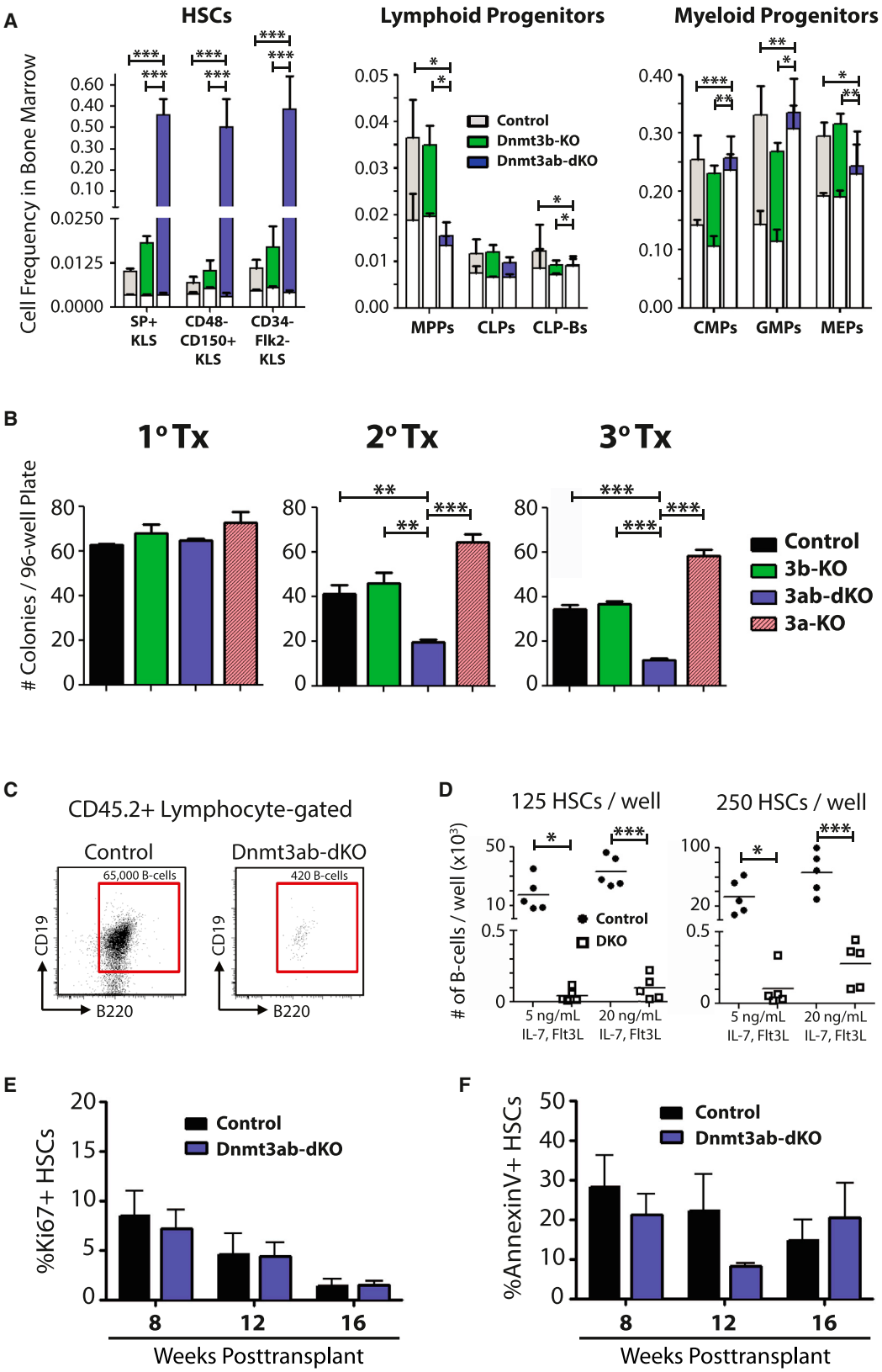

Figure 2. Dnmt3b Confers Some Differentiation Capacity in HSCs

(A) Frequencies of different cell compartments in the bone marrow of secondary recipient mice. White areas indicate the proportion of CD45.1$^+$ (competitor-derived) cells (n = 9–16). Statistical significance refers to comparisons of CD45.2$^+$ (donor-derived) populations.

(legend continued on next page)

DKO HSC Expansion Cannot Be Explained by Altered Proliferation or Apoptosis

To further investigate the mechanisms of DKO HSC accumulation in the bone marrow of transplant recipients, we performed a kinetic analysis of HSC proliferation and apoptosis at monthly intervals during secondary hematopoietic repopulation. At no time point did DKO HSCs exhibit greater proliferation (measured by Ki67 positivity) than control HSCs (Figure 2E), and both populations increasingly entered quiescence over time. DKO and control HSCs exhibited similar levels of AnnexinV staining, indicating that the accumulation of DKO HSCs cannot be attributed to apoptosis resistance (Figure 2F). Altogether, these data suggest that the accumulation of DKO HSCs is most likely a result of cell divisions that almost exclusively result in symmetric self-renewal rather than differentiation.

Ablation of *Dnmt3a* and *Dnmt3b* in HSCs Drive Localized DNA Methylation Loss

To address the epigenetic differences between Dnmt3 mutant HSCs, we performed whole-genome bisulfite sequencing (WGBS) of age-matched control versus tertiary-transplanted 3aKO and DKO HSCs. It was not possible to obtain sufficient 3bKO HSCs at the equivalent stage because of their limited expansion. These studies differed from our previous comparisons of control and 3aKO HSCs (Challen et al., 2012) in (1) comprehensive nature (WGBS instead of reduced representation bisulfite sequencing [RRBS]), (2) analysis at the tertiary rather than secondary transplant stage, given that that is when the DKO phenotype is most dramatic, and (3) control HSCs used were from age-matched, untransplanted control mice because of the limited number of posttransplant control HSCs obtainable.

We generated between 1.1 and 1.2 billion raw reads for each of three genotypes, covering nearly all 21 million CpGs in the mouse genome (mm9) with an average depth of 40× to 47× (Table S1). In comparison to control HSCs, 3aKO and DKO HSCs showed a global decrease in DNA methylation (average CpG methylation: 83.94% for control, 78.38% for 3aKO, and 78.01% for DKO; Figure 3A). Methylation was reduced across all genomic features (Table S1) and genic elements (Figure 3B). This contrast with our previous RRBS analysis, which indicated no significant difference between control and 3aKO HSCs (Challen et al., 2012), can be attributed to the bias of RRBS toward CpG-dense genomic regions. To control for possible transplantation effects on methylation (potentially masked by our use of untransplanted control HSCs), we examined the impact of transplantation as revealed by an independent study of aging HSCs (Beerman et al., 2013). Comparison of CpGs covered by both methods showed an average loss of DNA methylation of 11.8% in Dnmt3 mutant HSCs versus 6.9% because of transplantation as identified by Beerman et al. (2013). Thus, we cannot exclude some impact of transplantation itself, but the loss of *Dnmt3a/b* has a much greater impact.

This high-sequencing coverage allowed quantification of differential DNA methylation throughout specific genomic features, for which we defined a change of ±33% of DNA methylation (false discovery rate [FDR] < 0.05) as a differentially methylated CpG (DMC) (Gu et al., 2010). One of the genomic loci that showed the most dramatic DNA methylation changes was repetitive elements (Table S2), with 66% and 61% of DMCs within repeats in 3aKO and DKO HSCs, respectively, becoming hypomethylated (Figure S3A). This included repetitive elements targeted by the de novo DNA methyltransferases in ESCs (Figure S3B). This hypomethylation was often associated with increases in repeat expression (Figure S3C), reinforcing the notion that one role of the Dnmt3s is to silence these repetitive elements to safeguard the genome.

To examine whether ablation of the *Dnmt3*s affected DNA methylation in specific gene sets, DMCs were grouped into differentially methylated regions (DMRs), defined as at least three neighboring DMCs of the same class (see the Experimental Procedures). Because comparison of control versus mutant methylomes identified over 70,000 DMRs across the genome (Table S3), we initially focused on gene-associated DMRs (defined as being within a gene or 3 kb upstream of transcription start site or 3 kb downstream of transcription termination site). Respectively, 92.5% (9,353/10,110) and 95.6% (8,765/9,171) of DMRs in 3aKO and DKO HSCs became hypomethylated in comaprison to control HSCs (Table S3). Comparison of the DKO with the 3aKO revealed fewer DMRs (3,495), of which the majority showed a further loss of DNA methylation after additional loss of *Dnmt3b*. Most of the strongly hypomethylated DMRs were conserved between the two mutant HSC genotypes (Figure 3C).

The most striking difference between 3aKO and DKO HSCs was within CpG islands (CGIs). In comparison to control HSCs, 3aKO HSCs show a net gain of DNA methylation in CGIs, whereas DKO HSCs experience a net loss of DNA methylation like in other genomic features (Figure 3D). CGIs are the only definable class of elements in the genome that exhibit this dichotomy (Figure 3D). Although CpGs within loci groups such as "all" and "gene" contain similar proportions of hypomethylated DMCs in 3aKO and DKO HSCs, there is a strikingly less hypomethylation within CGIs from 3aKO HSC regardless of the genomic context of where the CGI is located (Figure 3E). Of the DMCs that were hypomethylated in both 3aKO and DKO HSCs, there was enrichment for the distribution of these CpGs within binding sites for transcription factors (TFs) important for HSC regulation (Wilson et al., 2010) (Figure 3F). This may provide an indirect mechanism for transcriptional changes in Dnmt3 mutant HSCs, as lower DNA methylation may influencing TF binding, although how these DNA methylation changes alter physical association of these sites with TFs remains to be

(B) Number of colonies generated per plate from HSCs at the end of each round of serial transplantation (n = 4). Single HSCs were sorted into individual wells of 96-well plates in Methocult media containing stem cell factor, IL-3, IL-6, and erythropoietin.
(C) Flow cytometric analysis of B cell differentiation from control and DKO HSCs in vitro.
(D) Numbers of B cells generated from control and DKO HSCs after 14-day culture (n = 5).
(F) Dynamic analysis of HSC proliferation during secondary hematopoietic reconstitution with Ki67 staining (n = 4).
(G) Dynamic analysis of HSC apoptosis during secondary hematopoietic reconstitution with AnnexinV staining (n = 3). Mean ± SEM values are shown. *p < 0.05, **p < 0.01, ***p < 0.001.
See also Figure S2.

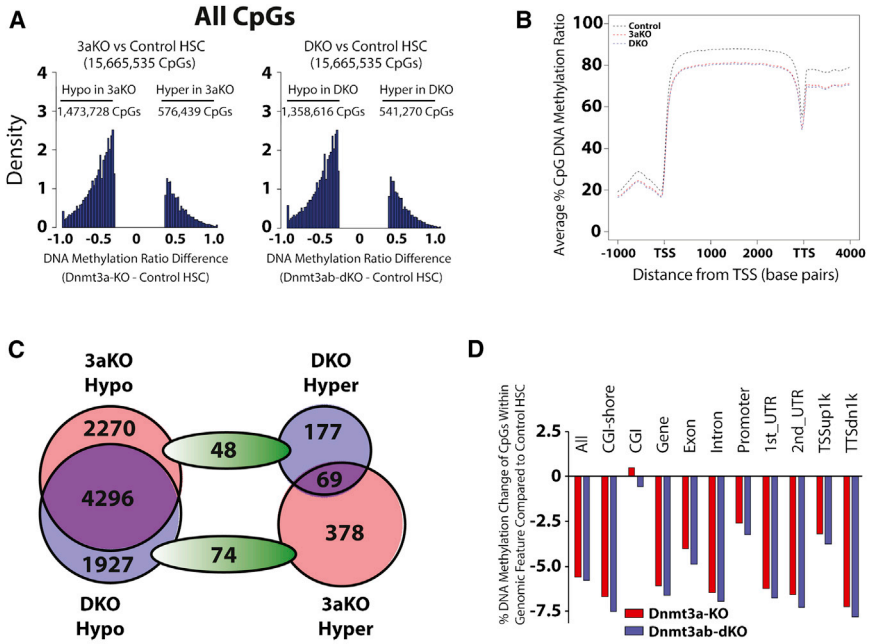

Figure 3. Global DNA Methylation Defects in Dnmt3 Mutant HSCs

(A) Distribution of all DMCs in the genome of Dnmt3 mutant HSCs relative to control from WGBS data.

(B) Average DNA methylation profile of CpGs across genic elements in control, 3aKO, and DKO HSCs.

(C) Distribution of DMCs within CGIs of Dnmt3 mutant HSCs compared to control.

(D) Average DNA methylation changes across genomic elements in Dnmt3 mutant HSCs relative to control.

(E) Percentages of hypomethylated DMCs within genomic elements in Dnmt3 mutant HSCs in comparison to control.

(F) Hypomethylated DMCs are enriched in transcription factor binding sites. Hypermethylated DMCs in 3aKO HSCs are enriched in CGIs.

See also Figure S3 and Tables S1, S2, and S3.

confirmed. The DMCs that were hypermethylated in 3aKO HSCs in comparison to both control and DKO HSCs were specifically enriched within CGIs (Figure 3F). These WGBS data suggest that, although the additional loss of *Dnmt3b* augments the global net loss of DNA methylation resulting from inactivation of *Dnmt3a*, Dnmt3b contributes to inappropriate hypermethylation of CGIs in in the absence of Dnmt3a.

We have recently shown that Dnmt3a maintains distinct subsets of large DNA methylation lacunae that we termed "canyons" (Jeong et al., 2014). To examine the impact of additional loss of *Dnmt3b* on canyons, we compared the sizes of the 3aKO canyons with DKO canyons. Of the canyons that previously contracted (largely harboring unexpressed genes), 78% now expand in DKO HSCs (Figure S3D). Similarly, 27% of the canyons that expanded in absence of *Dnmt3a* (harboring highly expressed genes) are further enlarged in the DKO (Figure S3D). These data demonstrate that like Dnmt3a, Dnmt3b is involved in canyon size maintenance. Canyon views also demonstrate the remarkable specificity of Dnmt3a and Dnmt3b action, exemplified by a distant perspective of the *Meis1* and *HoxA* loci, in which the associated canyon regions are eroded in 3aKO and DKO HSCs, but methylation loss outside these regions is minimal (Figures S3E and S3F).

Dnmt3a and *Dnmt3b* Combine to Epigenetically Repress the Stem Cell Gene Network during HSC Differentiation

To examine the effects of DNA methylation changes in 3aKO and DKO HSCs on gene expression, we performed RNA sequencing (RNA-seq) on the same cell populations used for WGBS. With a cutoff of FDR < 5%, there are 546 and 633 genes significantly upregulated and downregulated, respectively, in 3aKO HSCs in comparison to control HSCs (Table S4). Similarly, 549 and 514 genes were upregulated and downregulated, respectively, in DKO HSCs in comparison to control HSCs (Table S4). The majority of upregulated genes in 3aKO HSCs are also upregulated in DKO HSCs and vice versa (Figure 4A). Furthermore, KEGG pathway analysis showed many of the same functional categories enriched in both mutant genotypes, such as upregulation of TGFβ signaling. One divergence was that MAPK signaling was enriched in 3aKO HSCs, whereas Hedgehog signaling was enriched in DKO HSCs (Figure S4A). The genes downregulated in both mutant genotypes involved cell cycle, niche interactions, and hematopoietic lineage-specification programs (Figure S4B). Gene set enrichment analysis on the genes significantly differentially expressed in mutant HSCs correlated the genes upregulated in mutant HSCs with genes increased in cells after exposure to the demethylating agent 5-azacytidine (Figure S4C). There was no overlap between the genes upregulated in 3aKO HSCs and downregulated in DKO HSCs, and only four genes (*Atp7b*, *Krt8*, *Clec11a*, and *Mxra8*) that were downregulated in 3aKO HSCs but upregulated in DKO HSCs (Figure 4B). Some differences in the outlier genes can be explained by differential DNA methylation, such

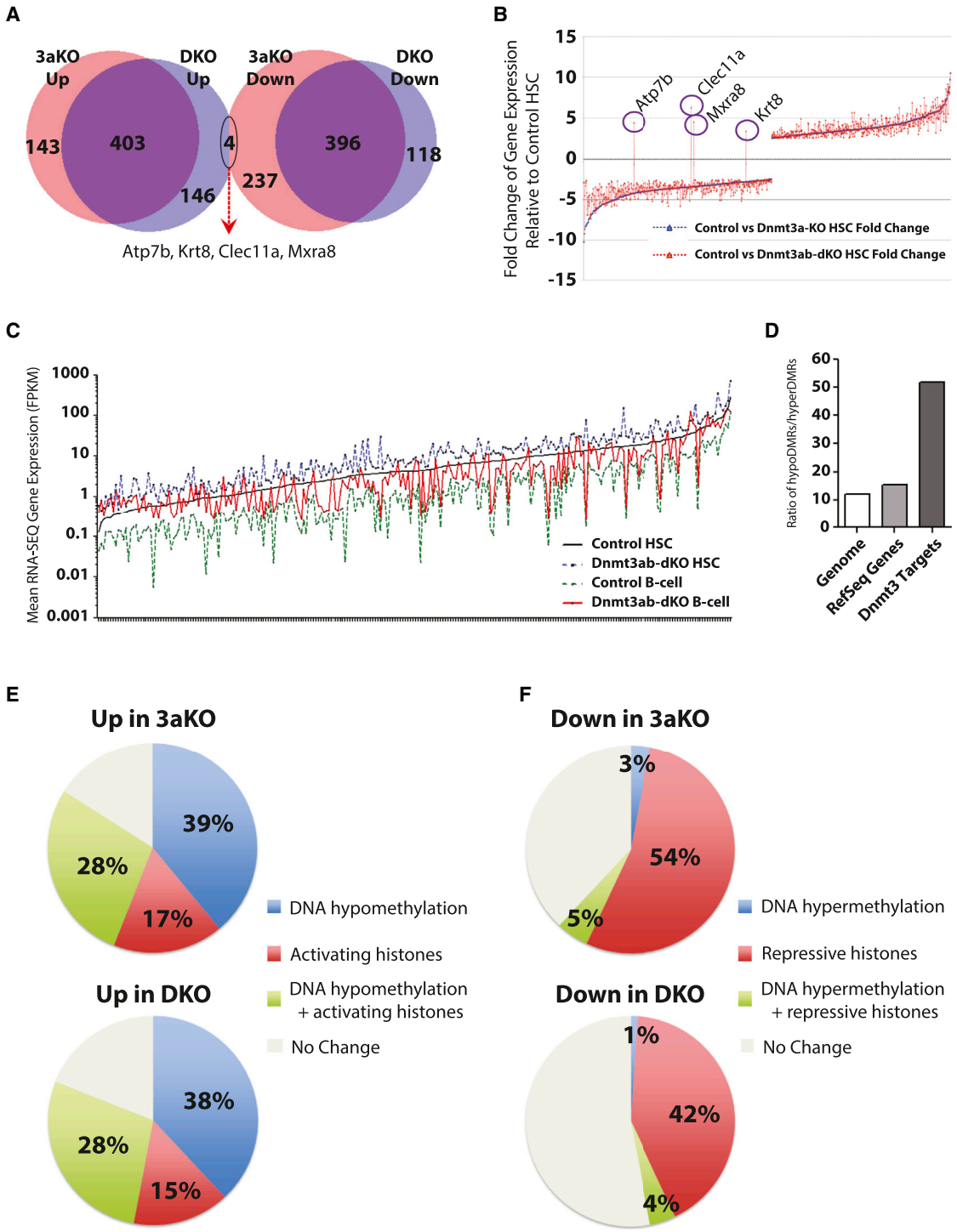

Figure 4. The Dnmt3s Repress HSC-Specific Genes and Gene Expression Changes Are Explained by Epigenetic Dynamics

(A) Overlap of differentially expressed genes between Dnmt3 mutant HSCs and control HSCs.

(B) Plotting fold change in transcript expression of genes differentially expressed between 3aKO and control HSCs as the baseline. Overlay of fold change in DKO HSCs relative to controls show a highly similar pattern.

(C) Identification of stem cell genes repressed by Dnmt3s during HSC differentiation. The baseline is RNA-seq expression of genes in control HSCs. Plot shows increased expression in DKO HSCs, repression in control B cells, and intermediate expression (incomplete repression) in DKO B cells.

(D) The ratio of hypomethylated DMRs to hypermethylated DMRs shows enrichment for hypomethylation of Dnmt3-regulated genes relative to the rest of the genome.

(legend continued on next page)

as *Krt8*, which, in 3aKO HSCs, has a hypermethylated DMR in exon 1 that is not present in control or DKO HSCs (Figure S4D).

We have previously shown that a major function of Dnmt3a in HSCs was to epigenetically repress the stem cell genetic network to downregulate HSC self-renewal genes and allow differentiation (Challen et al., 2012). To examine this model in an unbiased way in the DKO situation, we performed RNA-seq on control and DKO-derived B cells after secondary transplantation when some differentiation capacity remained. To identify epigenetically regulated genes, we selected genes that were upregulated >1.50-fold in DKO HSCs in comparison to control HSCs, in control HSCs in comparison to control B cells, and in DKO B cells in comparison to control B cells; this defined a cohort of 254 genes (Table S4). Setting the expression level of each gene in control HSCs as a baseline, all genes have increased expression in DKO HSCs and dramatically decreased expression in control B cells (Figure 4C). The role of the *Dnmt3*s in epigenetic repression of these stem-cell-specific genes is clear because the expression patterns for DKO B cells fall in between control HSCs and control B cells. Independent analysis of DNA methylation patterns of this cohort of 254 genes in DKO HSCs revealed that the ratio of hypomethylated to hypermethylated DMRs (compared to control HSCs) was 50-fold (Figure 4D), significantly greater than the average ratio throughout the genome or the average of all genes. Thus, in normal hematopoiesis, these genes are predominantly expressed in HSCs and are silenced by Dnmt3s during differentiation. In the absence of the Dnmt3s this process is inefficient, leading to enforced HSC self-renewal and incomplete repression of stem-cell-specific genes in differentiated progeny.

Differential Gene Expression Can Largely Be Explained by Epigenetic Dynamics

To gain insight into the influence of altered DNA methylation on other epigenetic marks, we performed chromatin immunoprecipitation (ChIP) sequencing (ChIP-seq) for the activating histone mark H3K4me3 and the repressive mark H3K27me3. We identified 14,494, 13,898, and 13,807 H3K4me3 peaks for control, 3aKO, and DKO HSCs, respectively, and 5,606, 4,358, and 6,531 H3K27me3 peaks for control, 3aKO, and DKO HSCs, respectively (Table S5) that were associated with gene promoters (±3 kb of transcription start site). By overlaying WGBS and ChIP-seq data, the majority of gene expression changes in mutant HSCs can be explained by epigenetic dynamics. Eighty four percent and 81% of the genes with significantly increased expression in 3aKO and DKO HSCs, respectively, contained a hypomethylated DMR, increased H3K4me3, decreased H3K27me3 (all epigenetic marks associated with increased gene expression), or some combination of the three epigenetic marks (Figures 4E and S4E). Conversely, 62% of the genes significantly downregulated in 3aKO HSCs were associated with an epigenetic mark more indicative of transcriptional repression—either a hypermethylated DMR, decreased H3K4me3, increased H3K27me3, or some combination (Figures 4F and S4E). However, only 47% of the downregulated genes could be explained by the same phenomena in DKO HSCs (Figure 4F). Although DNA hypomethylation was the major driver of increased gene expression in Dnmt3 mutant HSCs, loss of the H3K4me3 histone modification was more predictive of transcriptional repression than changes in DNA methylation. These altered epigenetic patterns had consequences for alternative promoter utilization, an example being *Tmcc3*, for which the longer isoform was exclusively observed in the mutant HSCs (Figure S4F). This suggests that the Dnmt3s and DNA methylation influences chromatin patterns to cooperatively control HSC self-renewal and differentiation cell fate decisions.

β-Catenin Signaling Contributes to the Block in DKO HSC Differentiation

Ingenuity pathway analysis (IPA) was used to highlight potential gene regulatory differences between 3aKO and DKO HSCs. IPA discriminated the β-catenin (*Ctnnb1*) pathway to be dramatically activated in DKO HSCs (the same pathway was slightly below the IPA threshold for being considered activated in 3aKO HSCs). *Ctnnb1* transcript expression was significantly increased in DKO HSCs (Figure 5A), and RNA-seq expression of validated β-catenin target genes such as *Ccnd1*, *Pparδ*, *Vegfα*, and *Jag1* was also significantly increased (Figure 5B). Mouse models in which HSCs constitutively express activated β-catenin show similar phenotypes to DKO HSCs, such as an 8- to 15-fold increase in the HSC pool and impaired differentiation in reconstitution assays (Scheller et al., 2006). We postulated that enhanced activity of this pathway may be responsible for some of the differentiation arrest of DKO HSCs.

DNA methylation analysis of the *Ctnnb1* locus identified a DKO hypomethylated region in the shore of the promoter CGI (Figure 5C). This created a new DNA methylation canyon (Figures 5D and S5A). Immunofluorescent staining of postsecondary transplant HSCs (Figure 5E) showed an increase in nuclear β-catenin in DKO HSCs (Figure S5B) as well as more total β-catenin protein (Figure S5C). On the basis of an arbitrary cutoff of 0.2 mean fluorescence units, 81% of DKO HSCs showed nuclear β-catenin in comparison to only 48% of control HSCs. To explore whether this contributed to the differentiation deficit of DKO HSCs, we ectopically expressed *Axin* in posttransplant HSCs. Expression of the Wnt pathway inhibitor Axin in HSCs reduces function by degrading β-catenin (Reya et al., 2003). Control and DKO bone marrow progenitors were transduced with control empty vector (MIG) or Axin-expressing (MIG-Axin) retrovirus and cultured for 2 days. Then, viable GFP^+ HSCs were purified ($Lin^-Sca\text{-}1^+c\text{-}Kit^+CD150^+$) and cocultured on OP9 stromal cells in lymphoid cytokines. Enumeration of $B220^+CD19^+$ cells after 14 days of coculture showed that ectopic Axin expression was able to partially rescue the in vitro B cell differentiation defect of DKO HSCs but did not affect the number of B cells generated from control HSCs (Figure 5F). We were able to elicit a similar response through knockdown of *Ctnnb1* transcript levels

(E and F) Categorical breakdown of genes differentially expressed in 3aKO and DKO HSCs in comparison to controls according to their epigenetic status. Increased gene expression in 3aKO and DKO HSCs is dominated by hypomethylation (E), whereas decreased gene expression is underpinned more by loss of activating chromatin (F). Activating histone, increased H3K4me3 and/or reduced H3K27me3. Repressive histones, decreased H3K4me3 and/or increased H3K27me3.

See also Figure S4 and Tables S4 and S5.

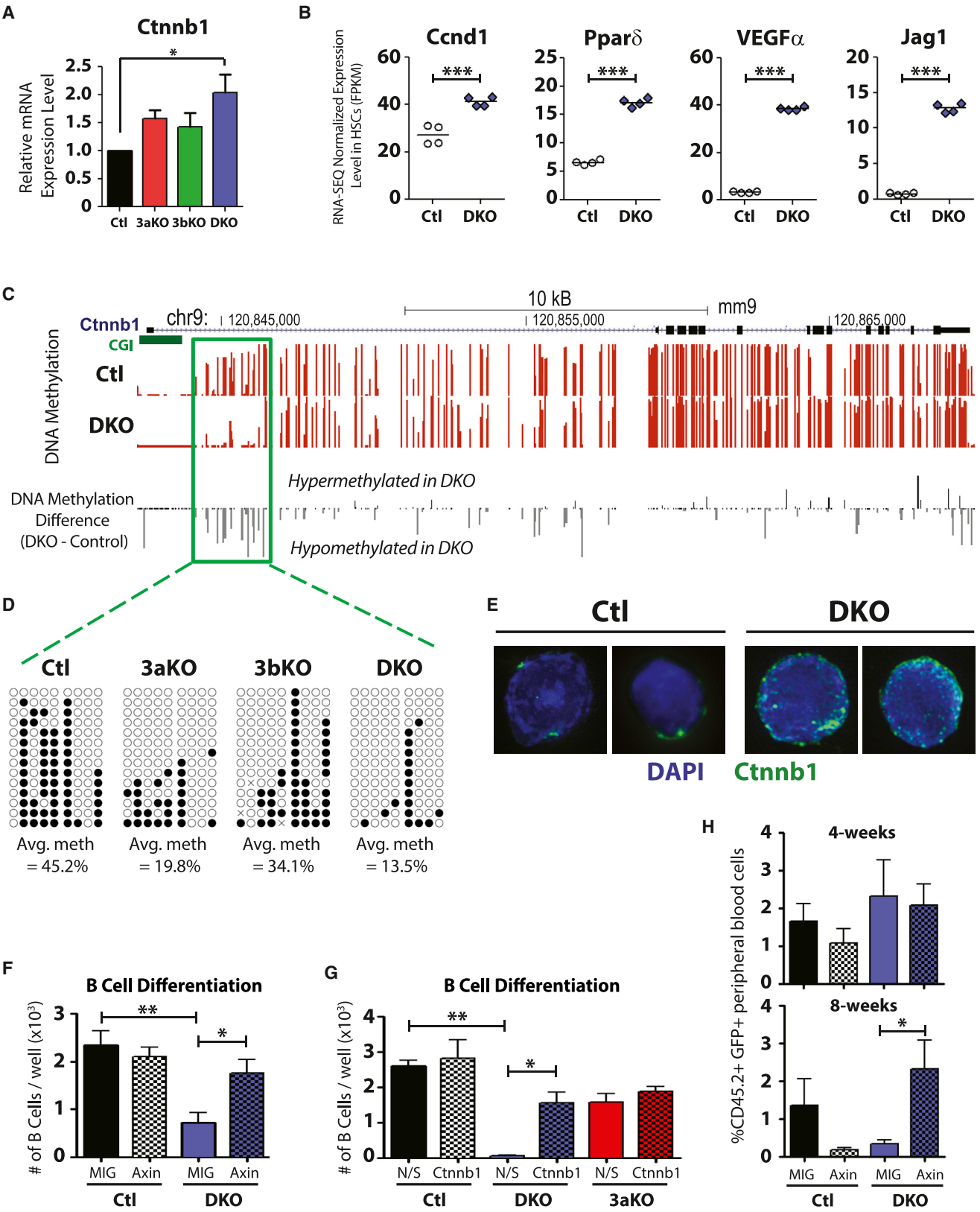

Figure 5. Increased β-Catenin Signaling Contributes to the Differentiation Block of DKO HSCs

(A) Real-time PCR analysis of *Ctnnb1* transcript expression in HSCs (n = 3).

(B) RNA-seq expression of Ctnnb1 target genes in control (Ctl) and DKO HSCs.

(legend continued on next page)

(Figure S5D), although this had no effect on the B cell potential of 3aKO HSCs (Figure 5G). Given that overexpression of Axin produced a similar response to *Ctnnb1* knockdown in terms of β-catenin target gene response (Figure S5E), we tested whether this strategy could also restore DKO HSC differentiation potential in vivo. Posttransplant HSCs were transduced with MIG and MIG-Axin and transplanted into lethally irradiated mice. Ectopic expression of Axin significantly enhanced peripheral blood differentiation of DKO HSCs 8 weeks posttransplant (Figure 5H). Altogether, these data strongly support the notion that the diminished differentiation activity of the DKO HSCs is due at least in part to persistent β-catenin activation.

Abnormal Dnmt3b Activity in the Absence of Dnmt3a Results in Aberrant CGI Hypermethylation

One puzzling observation was the finding that a specific subset of CGIs in HSCs actually showed increased DNA methylation levels after the ablation of *Dnmt3a*. Promoter CGI hypermethylation is a well-established cancer methylome phenotype (Figueroa et al., 2009; Shen et al., 2010, 2007), so this may be an important mechanism in the early stages of HSC transformation. In comparison to the control HSC methylome, 132 CGIs were significantly hypermethylated in 3aKO HSCs (Figure 6A and Table S6). The additional deletion of *Dnmt3b* abridged this effect, resulting in only 60 hypermethylated CGIs (Figure 6A). Sixty three CGIs were significantly hypermethylated in 3aKO HSCs in comparison to both control and DKO HSCs (Figure 6B). For genes with hypermethylated CGIs in the promoter region such as *Fam32a*, *Mpi*, and *Praf2*, this DNA hypermethylation was associated with gene repression (Figure 6C). One possibility was that this CGI hypermethylation was actually increased 5-hydroxymethylcytosine (5-hmC), and not 5-methylcytosine (5-mC) as bisulfite sequencing cannot discriminate between these epigenetic marks. We examined the 5-hmC pattern of the 63 hypermethylated CGIs with the use of 5-hmC profiles of control and 3aKO HSCs (Jeong et al., 2014). Only two of the 63 hypermethylated CGIs contained 5-hmC peaks in 3aKO HSCs (Figure S6A), suggesting that the majority of this hypermethylation was due to increased 5-mC. A recent epigenetic survey of ESCs deduced that CpG-dense promoters (such as those containing CGIs) are more likely to be repressed by the chromatin mark H3K27me3, whereas CpG-poor promoters are more likely to be epigenetically-regulated by DNA methylation (Xie et al., 2013). For the 63 CGIs that gain DNA methylation in 3aKO HSCs, 34 are marked by H3K27me3 in control HSCs, but only nine are marked in 3aKO HSCs (Figure S6B), suggesting that either of the two repressive marks was sufficient for silencing of the locus.

An alternative explanation suggested by these data is that in the absence of Dnmt3a, abnormal function of Dnmt3b, may lead to aberrant CGI hypermethylation as the hypermethylation was lost when both enzymes were inactivated. To explore this in HSCs, we analyzed DNA methylation patterns of tertiary transplant control, 3aKO, and 3bKO HSCs by RRBS (Table S6), which enriches for CGI-containing loci (Meissner et al., 2008). RRBS and WGBS showed strong concordance, and all 63 CGIs in 3aKO HSCs exhibit hypermethylation with both methods (Figure S6C). All of these CGIs were unmethylated in the control, 3bKO and DKO HSCs (Figure S6D), strongly suggesting that absence of Dnmt3a permits inappropriate Dnmt3b action.

To confirm this mechanism, posttransplant control and DKO bone marrow progenitors were transduced with a retroviral vector encoding full-length Dnmt3b (MIG-Dnmt3b1) or control (MIG). After 2 days, HSCs (GFP^+ $Lin^-Sca\text{-}1^+c\text{-}Kit^+CD150^+$ $CD45.2^+$) were purified and assessed for DNA methylation by bisulfite sequencing. Using the promoter CGI of *Praf2* as an example, hypermethylation is restricted to the 3aKO HSCs in comparison to control, 3bKO, and DKO genotypes (Figure 6D). Enforced expression of Dnmt3b1 in DKO HSCs resulted in increased DNA methylation at this locus in comparison to DKO HSCs transduced with MIG control, control HSCs transduced with either MIG or MIG-Dnmt3b1, and untransduced HSCs (Figure 6E). This indicates that, at least for some loci, in the absence of Dnmt3a, Dnmt3b functions abnormally in HSCs leading to aberrant CGI hypermethylation and anomalous gene silencing.

Dnmt3b Isoforms in HSC Function and Cancer

DNMT3A mutations are prevalent in a range of hematopoietic malignancies (Grossmann et al., 2013; Ley et al., 2010; Walter et al., 2011; Yan et al., 2011), a finding congruent with the differentiation arrest of mouse 3aKO HSCs. As we show Dnmt3b also plays a role in enabling differentiation, it is surprising only two *DNMT3B* point mutations have been reported in hematologic cancers to date (Cancer Genome Atlas Research Network, 2013). Over 30 different *Dnmt3b* isoforms resulting from alternative promoter usage or alternative splicing have been reported (Gopalakrishnan et al., 2009; Ostler et al., 2007; Xie et al., 1999). Spatiotemporal patterns of isoform expression are largely conserved between humans and mice (Okano et al., 1998), suggesting that these isoforms carry biological significance, even where splicing produces catalytically inactive proteins, such as mouse Dnmt3b3, which lacks the catalytic motifs encoded by exons 21 and 22. Moreover, transformation is known to change the complement of *DNMT3B* isoforms, with aberrant forms dominating in a number of malignancies (Ostler et al., 2007).

(C) DNA methylation profile of *Ctnnb1* locus determined by WGBS. The green box indicates hypomethylated region in DKO HSCs.
(D) Bisulfite sequencing of hypomethylated *Ctnnb1* region in HSC genotypes (open circle, unmethylated CpG; closed circle, methylated CpG).
(E) Immunofluorescent staining for Ctnnb1 (green) in control and DKO HSCs with DAPI staining (blue) defining the nucleus.
(F) Ectopic expression of Axin in DKO HSCs was able to partially rescue the B cell differentiation defect in comparison to DKO HSCs transduced with control retrovirus (MIG). Ectopic expression of Axin in Ctl HSCs did not affect B cell differentiation compared to MIG control cells (n = 4).
(G) miRNA-mediated knockdown of *Ctnnb1* was also able to restore B cell in DKO HSCs but had no effect on B cell differentiation of 3aKO HSCs (N/S, scrambled nonsilencing control miRNA; Ctnnb1, Ctnnb1 miRNA#1; n = 2).
(H) Peripheral blood chimerism following transduction and bone marrow transplant of control and DKO HSCs. Ectopic expression of Axin in DKO HSCs was able to significantly increase peripheral blood differentiation in comparison to the control MIG vector (n = 9–10 mice per group). Mean ± SEM values are shown. $^*p < 0.05$, $^{**}p < 0.01$.
See also Figure S5.

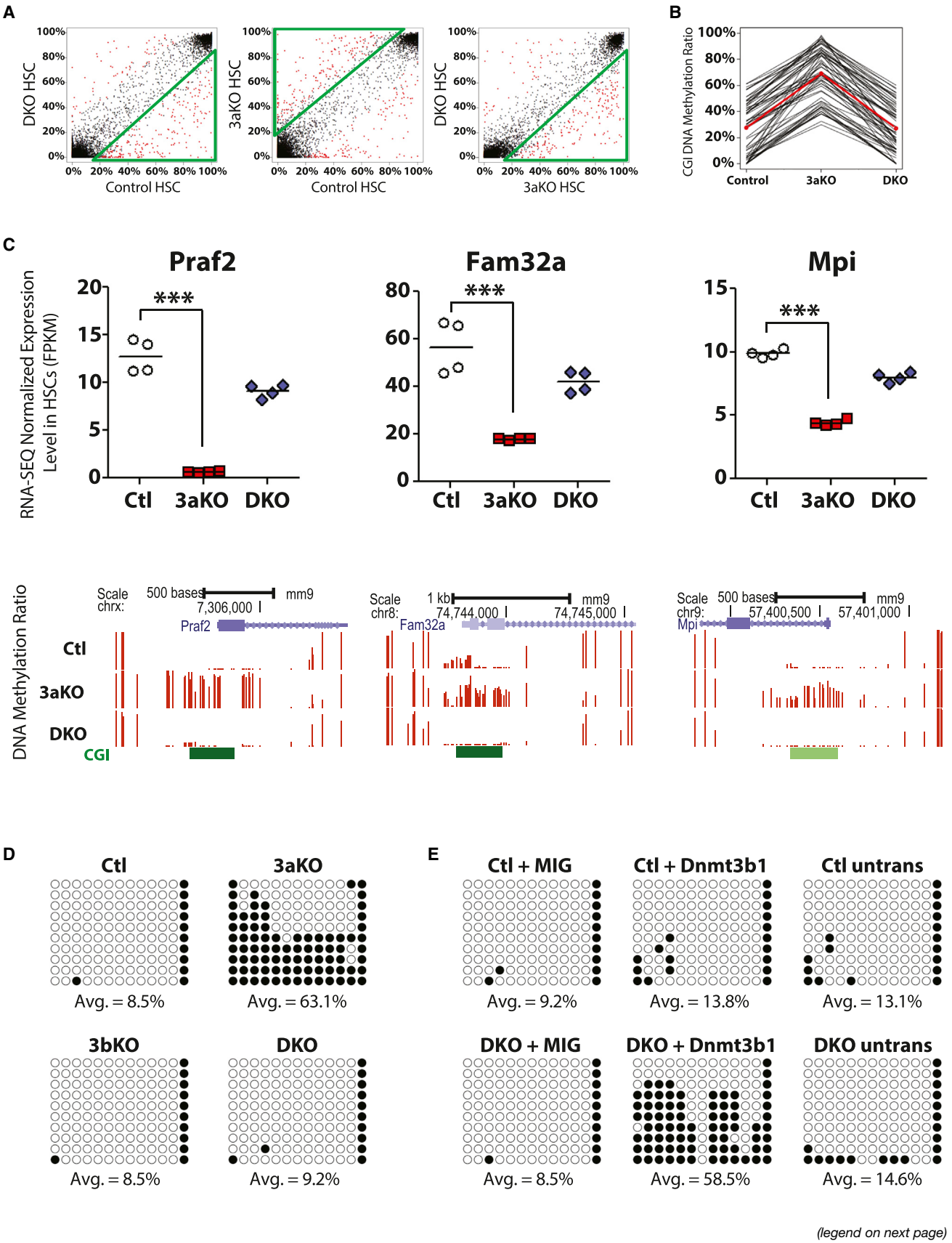

(legend on next page)

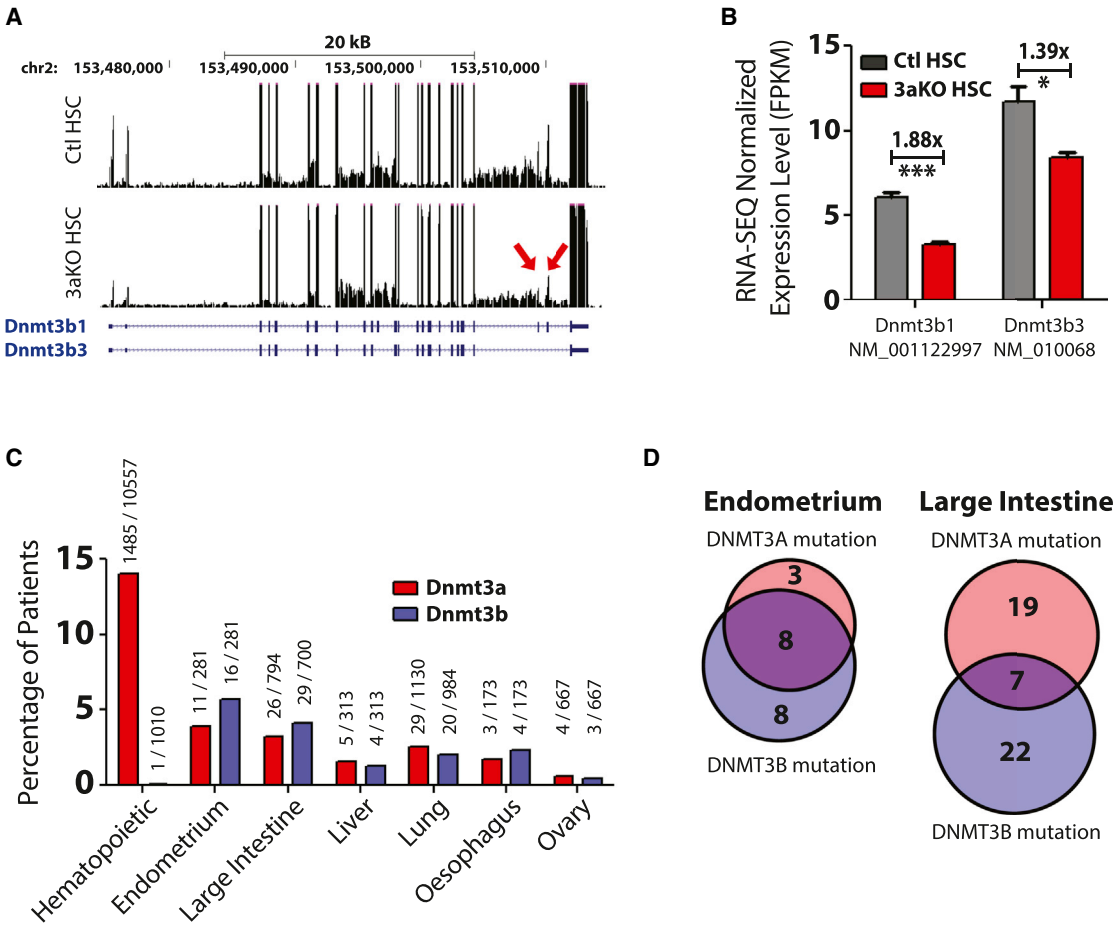

Figure 7. Dnmt3b Isoform Expression and Tumor Suppressor Role in HSCs

(A) RNA-seq expression of *Dnmt3b* isoforms in control (Ctl) and 3aKO HSCs. Exons 21 and 22 encoding the methyltransferase domain of *Dnmt3b1* are reduced in 3aKO HSCs.

(B) Ratio of *Dnmt3b* isoform expression in Ctl and 3aKO HSCs.

(C) Frequencies of genetic mutations in *DNMT3A* and *DNMT3B* in a range of tumors extracted from the COSMIC database.

(D) Overlap of *DNMT3* mutations in patients with endometrial and colon cancer in COSMIC database.

To consider these possibilities here, we examined the expression of *Dnmt3b* isoforms in RNA-seq data and found that only two *Dnmt3b* isoforms are expressed in control and 3aKO HSCs—*Dnmt3b1* and *Dnmt3b3* (Figure 7A). The predominant isoform was *Dnmt3b3*, which generates a catalytically inactive protein. This expression pattern is very similar to acute myeloid lymphoma patients harboring *DNMT3A* mutations (Cancer Genome Atlas Research Network, 2013). Although expression of both isoforms was slightly decreased in 3aKO HSCs in comparison to control (Figure 7B), there was a larger proportional decrease in *Dnmt3b1* levels in 3aKO HSCs. This suggests that there may be relatively little catalytically active Dnmt3b in normal HSCs, which is decreased even further after loss of Dnmt3a function. This most likely explains why 3bKO

Figure 6. CGI Hypermethylation in Dnmt3a-KO HSCs Is Mediated by Dnmt3b

(A) Comparison of differentially methylated CGIs across genotypes. Green triangles indicate the genotype with increased DNA methylation. Red dots indicate CGIs with statistically significant differences in DNA methylation.

(B) Identification of CGIs that are hypermethylated in 3aKO HSCs relative to control (Ctl) and DKO HSCs. Red line is the average DNA methylation profile.

(C) Gene expression and DNA methylation profiles of genes with hypermethylated promoter CGIs in 3aKO HSCs. Top, RNA-seq gene expression data; bottom, WGBS DNA methylation profiles. The height of each bar represents the DNA methylation level of an individual CpG.

(D) Promoter CGI DNA methylation profile of *Praf2* across HSC genotypes. Open circles represent unmethylated CpGs, and closed circles represent methylated CpGs.

(E) DNA methylation analysis of *Praf2* promoter by bisulfite PCR following transduction of Ctl or DKO HSCs with a control (MIG) or Dnmt3b-expressing (Dnmt3b1) retrovirus, compared to untransduced (untrans) HSCs. ***$p < 0.001$.

See also Figure S6 and Table S6.

alone has a relatively minor effect and why the phenotypes of the 3aKO and DKO HSCs are similar at both the phenotypic and molecular levels. Although the importance of Dnmt3b in HSCs is clear as even residual Dnmt3b1 activity is sufficient to maintain some differentiation capacity in 3aKO HSCs, similar to a recent study showing that in the absence of Dnmt3a, Dnmt3b functions as a tumor suppressor in chronic lymphocytic leukemia and T cell malignancies (Peters et al., 2014).

Given that *Dnmt3a* and *Dnmt3b* are broadly expressed during embryonic development (Okano et al., 1999), we considered the possibility that *DNMT3A* and *DNMT3B* mutations may play similar roles in other tissues. In the Catalogue of Somatic Mutations in Cancer (COSMIC) database (Bamford et al., 2004), *DNMT3B* mutations are detected in a range of solid tumors (Figure 7C) and often overlap with mutations in *DNMT3A* (Figure 7D). This suggests that in some tissues, compound inactivation of de novo DNA methylation facilitates transformation, possibly reflective of a different spectrum of *DNMT3B* isoforms expressed in these tissues. Although it is not possible to determine at this level of analysis whether *DNMT3A* and *DNMT3B* are drivers of these malignancies, given the data we present here, additional investigation is clearly warranted.

DISCUSSION

We have demonstrated here a specific role for Dnmt3b in permitting differentiation of HSCs. Although ablation of *Dnmt3b* alone in HSCs produces only a modest phenotype, the function of Dnmt3b is highlighted when inactivated in combination with Dnmt3a; the synergistic impact of the DKO would not be predicted from factorial enhancement of the individual KOs. A previous study reported de novo DNA methyltransferase activity was essential for self-renewal, given that *Dnmt3a*$^{fl/fl}$*Dnmt3b*$^{fl/fl}$ HSCs transduced with a Cre retrovirus could not sustain peripheral blood generation after bone marrow transplant (Tadokoro et al., 2007). We observe a similar effect of DKO on differentiation but also report extensive HSC expansion (self-renewal), which may have been missed previously because of the different experimental models (retroviral Cre and no serial transplantation).

When coupled with histone ChIP-seq analysis, a clear pattern for epigenetic regulation of gene expression in Dnmt3 mutant HSCs emerged. The genes upregulated in Dnmt3 mutant HSCs were underpinned by some combination of loss of DNA methylation (defined by the presence of a hypomethylated DMR) with a chromatin state more permissive for gene transcription (decreased H3K27me3 and/or increased H3K4me3). The genes downregulated in Dnmt3 mutant HSCs were not generally associated with changes in DNA methylation but rather dominated by changes in the histone code. Exactly how the chromatin architecture is instructed by the Dnmt3s remains to be determined. Possibilities include direct regulation of the writers and erasers of these marks by the Dnmt3s, recruitment of polycomb group proteins to epigenetic hotspots by the Dnmt3s or changes in DNA methylation patterns causing conformational changes to the chromatin that permits or inhibits access to other epigenetic regulators or transcription factors.

The Wnt/β-catenin pathway drives phenotypic HSC expansion by inducing proliferation while simultaneously inhibiting apoptosis and blocking differentiation (Perry et al., 2011), and sustained canonical Wnt signaling in HSCs through constitutively activated β-catenin causes a multilineage differentiation block (Kirstetter et al., 2006; Scheller et al., 2006) reminiscent of the Dnmt3 mutant HSC phenotype. Overexpression of Axin was able to partly restore the differentiation capacity of DKO HSCs, suggesting this pathway is a mechanism of HSC fate decisions that is under epigenetic control. However, in addition to *Ctnnb1*, there are surely other causative targets that contribute to the enhanced self-renewal and differentiation arrest of Dnmt3 mutant HSCs. For example, nuclear factor κB signaling regulates HSC self-renewal (Stein and Baldwin, 2013; Zhao et al., 2012), and *Nfkb2* is overexpressed ~4-fold in Dnmt3 mutant HSCs. Furthermore, loss of DNA methylation in TF binding sites after ablation of the *Dnmt3*s in HSCs (Figure 3F) may alter binding of master regulators such as Gata2, Runx1, Lmo2, and Scl, presenting an indirect mechanism with substantial downstream consequences.

With the mild in vivo phenotype of 3bKO HSCs, our data suggest Dnmt3a can compensate almost completely for Dnmt3b loss, but Dnmt3b is only partially able to reciprocate in the reverse situation. It is possible that the target specificity of the remaining catalytically functional Dnmt3b is distinct, leading to aberrant DNA methylation patterns such as CGI hypermethylation. On a gross level, the phenotypes of 3aKO and DKO HSCs are broadly similar. We propose this is because the predominant Dnmt3b isoform expressed in 3aKO HSCs is the catalytically inactive Dnmt3b3, resulting in quite minimal levels of de novo DNA methylation activity in 3aKO HSCs. Perhaps this explains the paucity of *DNMT3B* mutations in hematopoietic cancers because the relatively low level of catalytically competent DNMT3B means there is no selective pressure to genetically inactivate this gene after mutation of *DNMT3A*, with the *DNMT3A* mutant cancer cells functionally operating as a *DNMT3A/B* compound null. However, although the potency of Dnmt3b is less than Dnmt3a in HSCs, even residual levels of catalytic Dnmt3b clearly enable significant HSC differentiation, as even after three rounds of serial transplantation the self-renewal quotient of 3aKO HSCs is 5-fold less than that of DKO HSCs. The findings here build on the growing appreciation for epigenetic regulation in stem cell function. We show Dnmt3b has subtle, yet significant, roles in adult HSCs. Understanding the fundamental roles of Dnmt3s and DNA methylation in normal hematopoiesis is essential for deducing the impact of *DNMT3* mutations and altered DNA methylation patterns in cancer.

EXPERIMENTAL PROCEDURES

Animals

All animal procedures were approved by the International Animal Care and Use Committee and conducted in accordance the Baylor College of Medicine and Washington University in St. Louis institutional guidelines. All mice were C57Bl/6 background distinguished by CD45.1 or CD45.2 alleles. Dnmt3a$^{fl/fl}$ and Dnmt3b$^{fl/fl}$ mice were obtained from the Beaudet lab at Baylor College of Medicine (with the consent of En Li) and crossed to Mx1-Cre mice. For bone marrow transplantation, recipient C57Bl/6 CD45.1 mice were transplanted by retro-orbital injection after a split dose of 10.5 Gy of lethal

irradiation. 250 donor HSCs (CD45.2) were competed against 2.5 × 10^5 WBM cells with the opposite CD45 allele (matched to the recipient). In competitive transplantation experiments, deletion of floxed alleles in donor HSCs was mediated 5–6 weeks posttransplantation in primary recipients. Conditional deletion was mediated by six intraperitoneal injections (300 μg per mouse) of pIpC (Sigma-Aldrich) in PBS every other day. For serial HSC transplantation, WBM from transplanted recipients was isolated 18 weeks posttransplant, and donor HSCs were repurified with CD45.2$^+$SP^{KLS} gating. Of these repurified donor HSCs, 250 were competed against 2.5 × 10^5 fresh CD45.1 WBM. PCR screening of Dnmt3a and Dnmt3b floxed allele deletion was performed as previously described (Tadokoro et al., 2007).

Hematopoietic Stem Cell Purification and Flow Cytometry

For transplantation, HSCs were purified from the bone marrow with side population plus KLS (c-kit$^+$Lin$^-$Sca1$^+$) gating (see also the Supplemental Experimental Procedures). Bone marrow cells were stained for 90 min with Hoechst, magnetically enriched for c-Kit$^+$ cells, stained with additional antibodies, and then purified by flow cytometric cell sorting.

Whole-Genome Bisulfite Sequencing

Using a Covaris sonication system (Covaris S2), 300 ng genomic DNA was isolated and fragmented. Libraries were constructed with the Illumina TruSeq DNA sample preparation kit. After ligation, libraries were bisulfite-treated with the EpiTech Bisulfite Kit (QIAGEN). Ligation efficiency tested by PCR with TruSeq primers and Pfu Turbo Cx Hotstart DNA polymerase (Stratagene). After determining the optimized PCR cycle number for each samples, a large-scale PCR reaction (100 μl) was performed as described previously (Gu et al., 2011). PCR products were sequenced with Illumina HiSeq sequencing systems. WGBS data analyses were based on model-based analysis of bisulfite sequencing.

RNA-Seq

RNA was isolated from ~70,000 HSCs with the RNeasy Micro Kit (QIAGEN). Paired-end libraries were generated with Illumina TruSeq RNA sample preparation kit. Illumina HiSeq was used for sequencing with a paired-end sequencing length of 100 bp. The alignment was performed by RNA-seq unified mapper (RUM), which first mapped reads to the genome and transcriptome by Bowtie and then used blat to remap those initially unmapped reads to the genome. The information from the two rounds of mappings was merged. The multiply mapped reads were discarded. The gene annotations used for transcriptome alignment include RefSeq, University of California, Santa Cruz (UCSC) knownGene and ensemble gene models. The gene expression, fragments per kilobase of exon per million fragments mapped value, was calculated by counting the reads matching the exons of each gene. Differential expression was performed with edgeR.

ChIP-Seq

ChIP was performed with 50,000 HSCs. ChIPed DNA was purified with a MinElute Purification Kit (QIAGEN) and prepared for library construction using ThruPLEX-FD preparation kit without extra amplification (Rubicon). Sequencing was performed on a HiSeq 2000 (Illumina). Sequenced reads were mapped to the mm9 mouse genome and peaks were identified by model-based analysis of ChIP-seq data.

Statistical and Bioinformatic Analysis

See the Supplemental Experimental Procedures. All the RNA-seq, DNA methylation, and histone ChIP-seq data can be visualized on the UCSC Genome Browser at http://dldcc-web.brc.bcm.edu/lilab/deqiangs/dko/tracks.txt. Visit http://genome.ucsc.edu/cgi-bin/hgTracks?db=mm9&hubUrl=http://dldcc-web.brc.bcm.edu/lilab/deqiangs/dko/tracks.txt to visualize the trackhub.

ACCESSION NUMBER

All data have been uploaded to the NCBI Gene Expression Omnibus under accession number GSE50793.

SUPPLEMENTAL INFORMATION

Supplemental Information contains Supplemental Experimental Procedures, six figures, and six tables and can be found with this article online at http://dx.doi.org/10.1016/j.stem.2014.06.018.

AUTHOR CONTRIBUTIONS

G.A.C., A.M., M.L., M.J., C.M., L.Y., S.C., G.J.D., and M.A.G. designed and performed experiments. G.A.C., D.S., B.R., Z.X., W.L., and M.A.G. analyzed data. G.A.C. and M.A.G. wrote and edited the paper.

ACKNOWLEDGMENTS

We thank members of the G.A.C., W.L., and M.A.G. labs for helpful discussions. This work was supported by NIH grants DK084259, AG036562, CA126752, DK092883, CA125123, and AI07495 as well as the Ellison Medical Foundation, CPRIT grant RP110028, the Samuel Waxman foundation, and grants CPRIT RP110471 and NIH R01HG007538 to W.L.

Received: December 16, 2013
Revised: May 28, 2014
Accepted: June 23, 2014
Published: August 14, 2014

REFERENCES

Bamford, S., Dawson, E., Forbes, S., Clements, J., Pettett, R., Dogan, A., Flanagan, A., Teague, J., Futreal, P.A., Stratton, M.R., and Wooster, R. (2004). The COSMIC (Catalogue of Somatic Mutations in Cancer) database and website. Br. J. Cancer *91*, 355–358.

Beerman, I., Bock, C., Garrison, B.S., Smith, Z.D., Gu, H., Meissner, A., and Rossi, D.J. (2013). Proliferation-dependent alterations of the DNA methylation landscape underlie hematopoietic stem cell aging. Cell Stem Cell *12*, 413–425.

Bestor, T.H. (1992). Activation of mammalian DNA methyltransferase by cleavage of a Zn binding regulatory domain. EMBO J. *11*, 2611–2617.

Cancer Genome Atlas Research Network (2013). Genomic and epigenomic landscapes of adult de novo acute myeloid leukemia. N. Engl. J. Med. *368*, 2059–2074.

Challen, G.A., Sun, D., Jeong, M., Luo, M., Jelinek, J., Berg, J.S., Bock, C., Vasanthakumar, A., Gu, H., Xi, Y., et al. (2012). Dnmt3a is essential for hematopoietic stem cell differentiation. Nat. Genet. *44*, 23–31.

Chen, T., Ueda, Y., Dodge, J.E., Wang, Z., and Li, E. (2003). Establishment and maintenance of genomic methylation patterns in mouse embryonic stem cells by Dnmt3a and Dnmt3b. Mol. Cell. Biol. *23*, 5594–5605.

Dodge, J.E., Okano, M., Dick, F., Tsujimoto, N., Chen, T., Wang, S., Ueda, Y., Dyson, N., and Li, E. (2005). Inactivation of Dnmt3b in mouse embryonic fibroblasts results in DNA hypomethylation, chromosomal instability, and spontaneous immortalization. J. Biol. Chem. *280*, 17986–17991.

Figueroa, M.E., Skrabanek, L., Li, Y., Jiemjit, A., Fandy, T.E., Paietta, E., Fernandez, H., Tallman, M.S., Greally, J.M., Carraway, H., et al. (2009). MDS and secondary AML display unique patterns and abundance of aberrant DNA methylation. Blood *114*, 3448–3458.

Gopalakrishnan, S., Van Emburgh, B.O., Shan, J., Su, Z., Fields, C.R., Vieweg, J., Hamazaki, T., Schwartz, P.H., Terada, N., and Robertson, K.D. (2009). A novel DNMT3B splice variant expressed in tumor and pluripotent cells modulates genomic DNA methylation patterns and displays altered DNA binding. Mol. Cancer Res. *7*, 1622–1634.

Grossmann, V., Haferlach, C., Weissmann, S., Roller, A., Schindela, S., Poetzinger, F., Stadler, K., Bellos, F., Kern, W., Haferlach, T., et al. (2013). The molecular profile of adult T-cell acute lymphoblastic leukemia: mutations in RUNX1 and DNMT3A are associated with poor prognosis in T-ALL. Genes Chromosomes Cancer *52*, 410–422.

Gu, H., Bock, C., Mikkelsen, T.S., Jäger, N., Smith, Z.D., Tomazou, E., Gnirke, A., Lander, E.S., and Meissner, A. (2010). Genome-scale DNA methylation

mapping of clinical samples at single-nucleotide resolution. Nat. Methods *7*, 133–136.

Gu, H., Smith, Z.D., Bock, C., Boyle, P., Gnirke, A., and Meissner, A. (2011). Preparation of reduced representation bisulfite sequencing libraries for genome-scale DNA methylation profiling. Nat. Protoc. *6*, 468–481.

Hata, K., Okano, M., Lei, H., and Li, E. (2002). Dnmt3L cooperates with the Dnmt3 family of de novo DNA methyltransferases to establish maternal imprints in mice. Development *129*, 1983–1993.

Jaenisch, R., and Jähner, D. (1984). Methylation, expression and chromosomal position of genes in mammals. Biochim. Biophys. Acta *782*, 1–9.

Jeong, M., Sun, D., Luo, M., Huang, Y., Challen, G.A., Rodriguez, B., Zhang, X., Chavez, L., Wang, H., Hannah, R., et al. (2014). Large conserved domains of low DNA methylation maintained by Dnmt3a. Nat. Genet. *46*, 17–23.

Kirstetter, P., Anderson, K., Porse, B.T., Jacobsen, S.E., and Nerlov, C. (2006). Activation of the canonical Wnt pathway leads to loss of hematopoietic stem cell repopulation and multilineage differentiation block. Nat. Immunol. *7*, 1048–1056.

Lei, H., Oh, S.P., Okano, M., Jüttermann, R., Goss, K.A., Jaenisch, R., and Li, E. (1996). De novo DNA cytosine methyltransferase activities in mouse embryonic stem cells. Development *122*, 3195–3205.

Ley, T.J., Ding, L., Walter, M.J., McLellan, M.D., Lamprecht, T., Larson, D.E., Kandoth, C., Payton, J.E., Baty, J., Welch, J., et al. (2010). DNMT3A mutations in acute myeloid leukemia. N. Engl. J. Med. *363*, 2424–2433.

Li, E., Bestor, T.H., and Jaenisch, R. (1992). Targeted mutation of the DNA methyltransferase gene results in embryonic lethality. Cell *69*, 915–926.

Meissner, A., Mikkelsen, T.S., Gu, H., Wernig, M., Hanna, J., Sivachenko, A., Zhang, X., Bernstein, B.E., Nusbaum, C., Jaffe, D.B., et al. (2008). Genome-scale DNA methylation maps of pluripotent and differentiated cells. Nature *454*, 766–770.

Ng, H.H., and Bird, A. (1999). DNA methylation and chromatin modification. Curr. Opin. Genet. Dev. *9*, 158–163.

Okano, M., Xie, S., and Li, E. (1998). Cloning and characterization of a family of novel mammalian DNA (cytosine-5) methyltransferases. Nat. Genet. *19*, 219–220.

Okano, M., Bell, D.W., Haber, D.A., and Li, E. (1999). DNA methyltransferases Dnmt3a and Dnmt3b are essential for de novo methylation and mammalian development. Cell *99*, 247–257.

Ostler, K.R., Davis, E.M., Payne, S.L., Gosalia, B.B., Expósito-Céspedes, J., Le Beau, M.M., and Godley, L.A. (2007). Cancer cells express aberrant DNMT3B transcripts encoding truncated proteins. Oncogene *26*, 5553–5563.

Perry, J.M., He, X.C., Sugimura, R., Grindley, J.C., Haug, J.S., Ding, S., and Li, L. (2011). Cooperation between both Wnt/beta-catenin and PTEN/PI3K/Akt signaling promotes primitive hematopoietic stem cell self-renewal and expansion. Genes Dev. *25*, 1928–1942.

Peters, S.L., Hlady, R.A., Opavska, J., Klinkebiel, D., Pirruccello, S.J., Talmon, G.A., Sharp, J.G., Wu, L., Jaenisch, R., Simpson, M.A., et al. (2014). Tumor suppressor functions of Dnmt3a and Dnmt3b in the prevention of malignant mouse lymphopoiesis. Leukemia *28*, 1138–1142.

Reya, T., Duncan, A.W., Ailles, L., Domen, J., Scherer, D.C., Willert, K., Hintz, L., Nusse, R., and Weissman, I.L. (2003). A role for Wnt signalling in self-renewal of haematopoietic stem cells. Nature *423*, 409–414.

Scheller, M., Huelsken, J., Rosenbauer, F., Taketo, M.M., Birchmeier, W., Tenen, D.G., and Leutz, A. (2006). Hematopoietic stem cell and multilineage defects generated by constitutive beta-catenin activation. Nat. Immunol. *7*, 1037–1047.

Shen, L., Kondo, Y., Guo, Y., Zhang, J., Zhang, L., Ahmed, S., Shu, J., Chen, X., Waterland, R.A., and Issa, J.P. (2007). Genome-wide profiling of DNA methylation reveals a class of normally methylated CpG island promoters. PLoS Genet. *3*, 2023–2036.

Shen, L., Kantarjian, H., Guo, Y., Lin, E., Shan, J., Huang, X., Berry, D., Ahmed, S., Zhu, W., Pierce, S., et al. (2010). DNA methylation predicts survival and response to therapy in patients with myelodysplastic syndromes. J. Clin. Oncol. *28*, 605–613.

Stein, S.J., and Baldwin, A.S. (2013). Deletion of the NF-κB subunit p65/RelA in the hematopoietic compartment leads to defects in hematopoietic stem cell function. Blood *121*, 5015–5024.

Surani, M.A. (1998). Imprinting and the initiation of gene silencing in the germ line. Cell *93*, 309–312.

Tadokoro, Y., Ema, H., Okano, M., Li, E., and Nakauchi, H. (2007). De novo DNA methyltransferase is essential for self-renewal, but not for differentiation, in hematopoietic stem cells. J. Exp. Med. *204*, 715–722.

Walter, M.J., Ding, L., Shen, D., Shao, J., Grillot, M., McLellan, M., Fulton, R., Schmidt, H., Kalicki-Veizer, J., O'Laughlin, M., et al. (2011). Recurrent DNMT3A mutations in patients with myelodysplastic syndromes. Leukemia *25*, 1153–1158.

Wilson, N.K., Foster, S.D., Wang, X., Knezevic, K., Schütte, J., Kaimakis, P., Chilarska, P.M., Kinston, S., Ouwehand, W.H., Dzierzak, E., et al. (2010). Combinatorial transcriptional control in blood stem/progenitor cells: genome-wide analysis of ten major transcriptional regulators. Cell Stem Cell *7*, 532–544.

Wu, H., Coskun, V., Tao, J., Xie, W., Ge, W., Yoshikawa, K., Li, E., Zhang, Y., and Sun, Y.E. (2010). Dnmt3a-dependent nonpromoter DNA methylation facilitates transcription of neurogenic genes. Science *329*, 444–448.

Xie, S., Wang, Z., Okano, M., Nogami, M., Li, Y., He, W.W., Okumura, K., and Li, E. (1999). Cloning, expression and chromosome locations of the human DNMT3 gene family. Gene *236*, 87–95.

Xie, W., Schultz, M.D., Lister, R., Hou, Z., Rajagopal, N., Ray, P., Whitaker, J.W., Tian, S., Hawkins, R.D., Leung, D., et al. (2013). Epigenomic analysis of multilineage differentiation of human embryonic stem cells. Cell *153*, 1134–1148.

Yan, X.J., Xu, J., Gu, Z.H., Pan, C.M., Lu, G., Shen, Y., Shi, J.Y., Zhu, Y.M., Tang, L., Zhang, X.W., et al. (2011). Exome sequencing identifies somatic mutations of DNA methyltransferase gene DNMT3A in acute monocytic leukemia. Nat. Genet. *43*, 309–315.

Zhao, C., Xiu, Y., Ashton, J., Xing, L., Morita, Y., Jordan, C.T., and Boyce, B.F. (2012). Noncanonical NF-κB signaling regulates hematopoietic stem cell self-renewal and microenvironment interactions. Stem Cells *30*, 709–718.